

Computational Fluid Dynamic Model of a Commercial Atmospheric Pressure Ion Source

Thorsten Poehler²; Robert Kunte²; Herwart Hoenen²; Peter Jeschke²; Walter Wissdorf¹; Thorsten Benter¹

Introduction

The motion of ions at atmospheric pressure is governed by electrical field- and viscous drag-forces to a comparable extent.

Thus a comprehensive description of the conditions in an atmospheric pressure ion source has to incorporate the - in many cases very complex - bulk gas flows in the source geometry.

Numerical methods, in particular modern computational fluid dynamics (CFD) solver systems, are the tools of choice to simulate the gas flow in AP ion sources. Rigorous application of these methods could result in an important step forward on the way from trial-and-error towards model driven design approaches for new AP ion source geometries.

From our latest research efforts (see poster 070 in session TP04 for details) we propose that such a model driven design process is possible and feasible.

To analyze the current state of the technology and to proof that CFD is a useful tool even for complex fluid dynamical problems, we simulated the gas flow in a commercially available AP ion source (Bruker MPIS) and validated the flow simulations with appropriate experimental methods.

In this contribution we present the actual flow simulation, an experimental verification, and a detailed discussion of the results.

Methods

Numerical Methods

CFD solver:

Ansys CFX v. 12.0

Turbulence model:

Shear-Stress-Transport (SST) turbulence model

Analyte gas transport:

convection / diffusion equation

Experimental Methods

Particle Image Velocimetry Setup:

System: 2D PIV (LaVision, Goettingen, Germany)
Laser: New Wave 120 mJ YAG double pulse laser (ESI, Portland, USA)
PIV camera: dual frame technology, 12 bit, 1376 x 1040 Pixel (LaVision, Goettingen, Germany)
Seeding generator: DEHS oil, >108 particles/cm³ (Topas, Dresden, Germany)

Operating point adjustment:

Volume flows, pressures and temperatures were measured for calculation of the corresponding mass flows.
Volume flow meters: (MCC, Dortmund, Germany)

Ion Source Chamber:

Bruker multipurpose ion source (MPIS)

The modeled Ion Source

Operating conditions:

	OP _{V1}	OP _{I1}
Inflow Analyte:		
Mass flow [g s ⁻¹]	0.04	0.024
Total temperature [°C]	20	183
Turbulence intensity [%]	1	1
Analyte concentration [-]	1	1
Inflow Dry-gas:		
Mass flow [g s ⁻¹]	4.7	3.337
Total temperature [°C]	20	131
Turbulence intensity [%]	5	5
Analyte concentration [-]	0	0
Outflow MS:		
Static Pressure [kPa]	-93	-93
Outflow MS:		
Static Pressure [kPa]	100	100

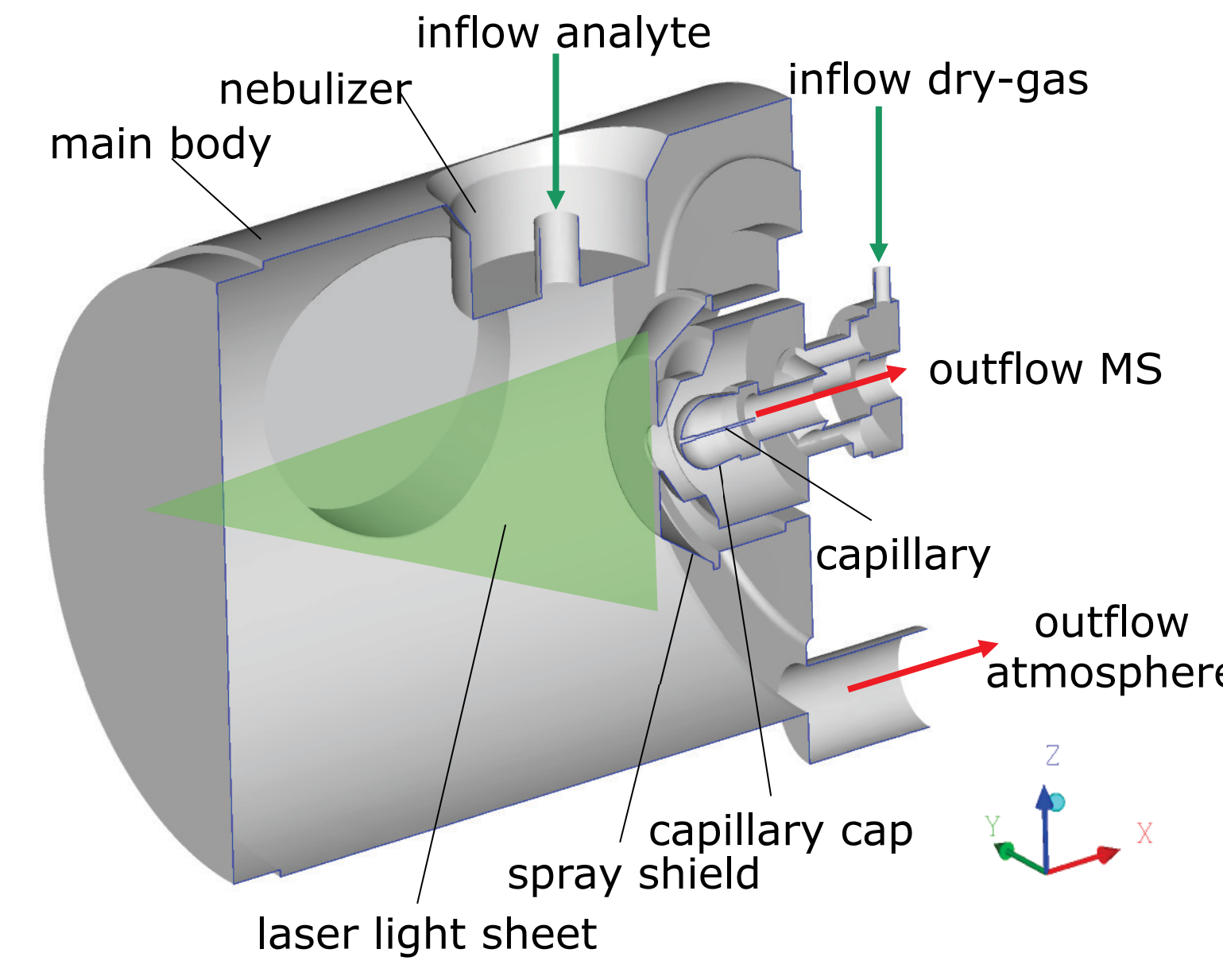


Figure 1) Schematic of the ion source (MPIS)

Particle Image Velocimetry (PIV)

The PIV measurement technique

Particle Image Velocimetry (PIV) measurements were conducted in order to obtain experimental validation data for the simulation runs. PIV is a laser-optical measurement technique which allows the collection of 2D velocity flow field data. Seeding oil drops are injected into the flow and illuminated by a laser light sheet in the measurement area. A fast CCD-camera gathers two pictures from which the flow field is calculated.

Figure 2 shows a photograph of the mass spectrometer inlet stage comprised of the MPIS, the desolvation unit, and a high vacuum chamber, cf. Figure 2b. This system mimics the analyzer inlet stage of the Bruker micrOTOF mass spectrometer series. The ionization chamber with the access for the analyte inflow via pneumatically assisted nebulization is seen in the center.

The light sheet optics and the PIV camera are positioned in a 90° angle around the chamber. The optics generate a light sheet of 1mm thickness with the focus in the measurement plane in front of the spray shield. The light sheet enters the chamber through a glass window. A black paper cylinder between the light sheet optics and the window is used for laser stray light protection.

The optical access for the camera is a glass window at the side of the chamber. The chamber is blackened to avoid laser reflections which would disturb the particle image capture. For calibration, a plate with a defined pattern is introduced into the measurement plane. The calibration function and scaling factors are calculated by the system software.

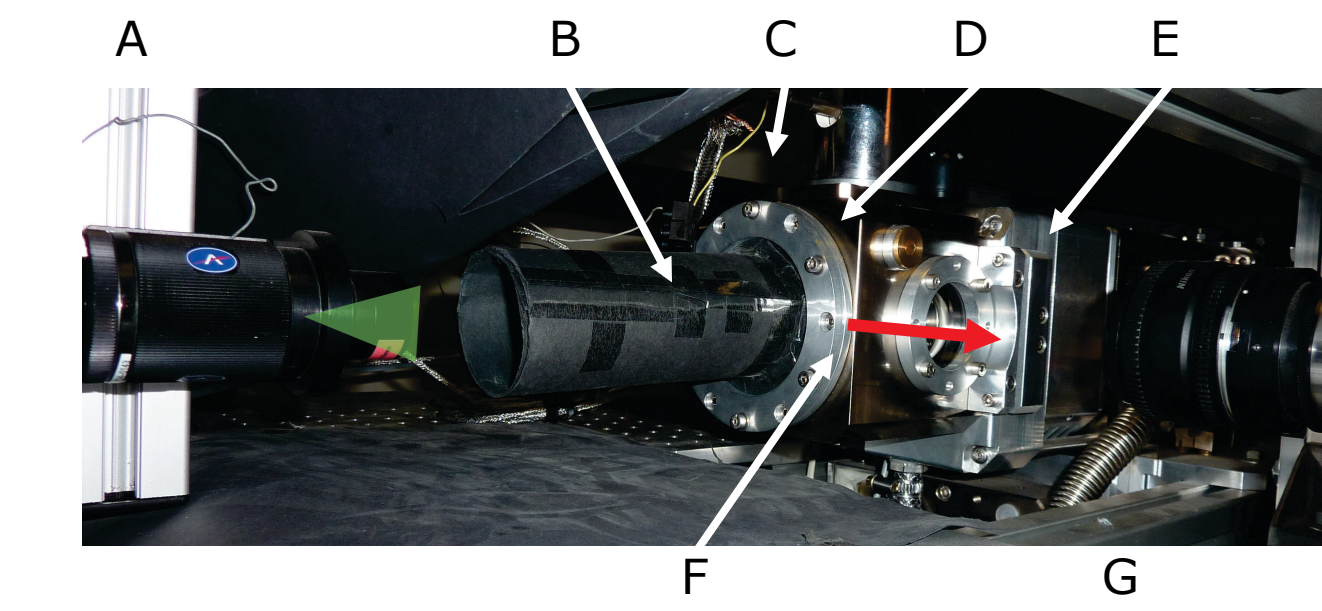


Figure 2) Adaptation of the PIV measurement technique.

A: Light sheet optics.
B: Light sheet access.
C: Inflow analyte.
D: MPIS.
E: MS desolvation stage followed by high vacuum stage.
F: Optical access.
G: PIV camera objective.
Green arrow: Light sheet direction;
Red arrow: Detection light direction.

CFD Validation / Comparison CFD - PIV

Mean Flow Field

Contour plots and streamlines of the velocity are presented in figure 3. In terms of the overall velocity vector field, numerical and experimental results are in very good agreement at both operating points. However, there are some subtle differences in the flow field.

Considering the analyte gas jet, the main difference is found in the width of the jet. The analyte jet is significantly wider in the numerical results. The discretization error resulting from a coarse grid in this region elevates an artificial (numerical) diffusion. The strong gradients at the edge of the jet cannot be resolved by the large finite volumes in this region, which then leads to a numerical diffusion.

The inclined flow angle of the dry-gas jet differs slightly, which is due to a different mass flow distribution in the dry gas connector. A lower backpressure at the numerical capillary outflow in the CFD simulations could improve the conformity with the experimental results concerning the velocity level and the flow angle of the jet.

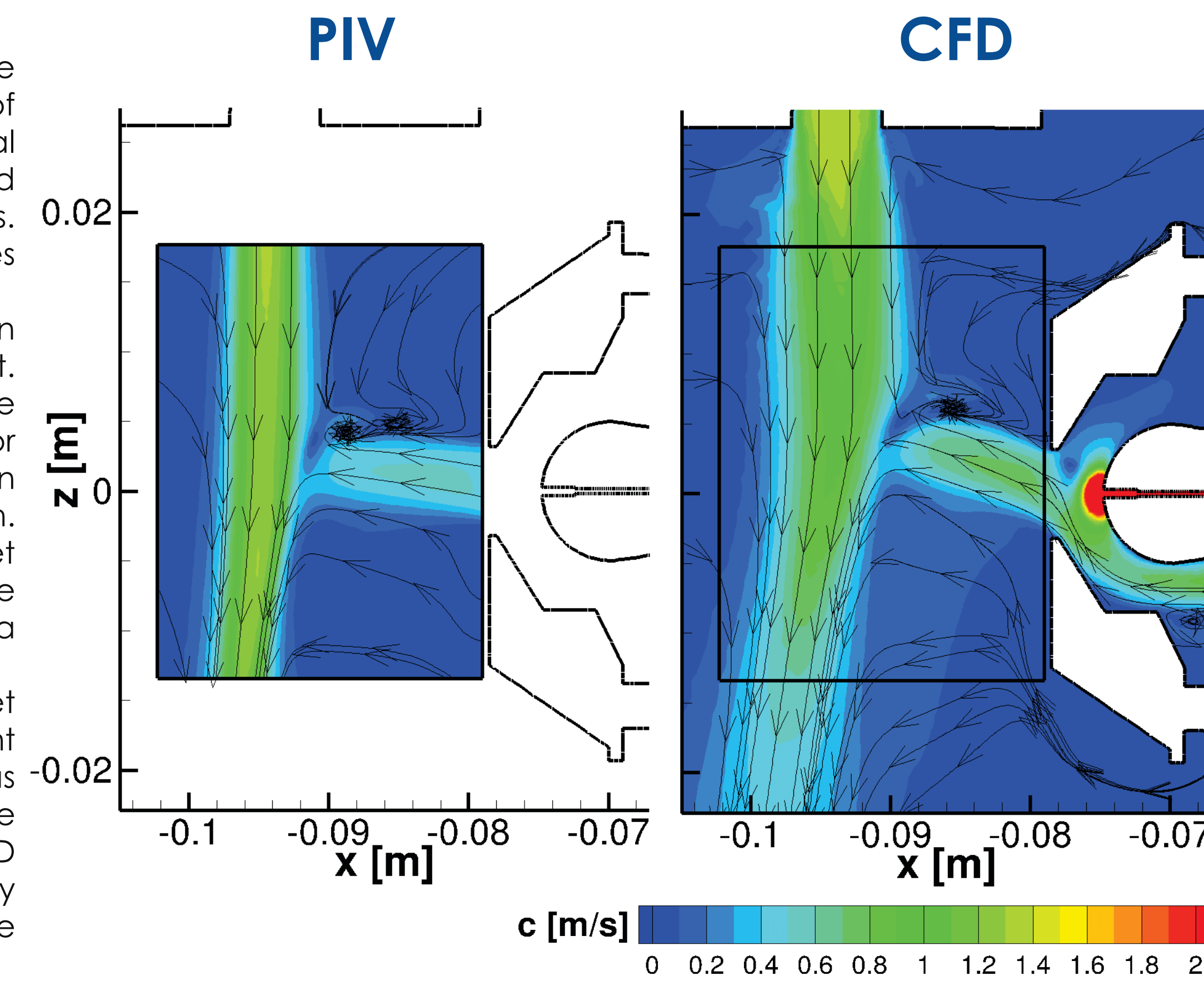


Figure 3) 2D velocity (PIV vs. CFD)

Two-dimensional Turbulence

Turbulence can be considered as a three-dimensional fluctuation of a flow quantity around a mean value. Due to the measurement technique only two dimensions of the turbulence have been resolved. The numerical solutions have been conducted with an isotropic turbulence model, therefore the two-dimensional turbulent kinetic energy is only 2/3 of the corresponding value of a three-dimensional turbulence.

In figure 4 the turbulent kinetic energy distribution is presented. The overall turbulent kinetic energy (TKE) is very low. An increase of the TKE is observed in the region where both components of turbulent fluctuations are of a significant magnitude. In the numerical results an additional spot of higher TKE at (x;z) = -0.087;0.007 occurs. This hot spot is generated by a vortex, which is discussed in the section "Neutral Analyte distribution".

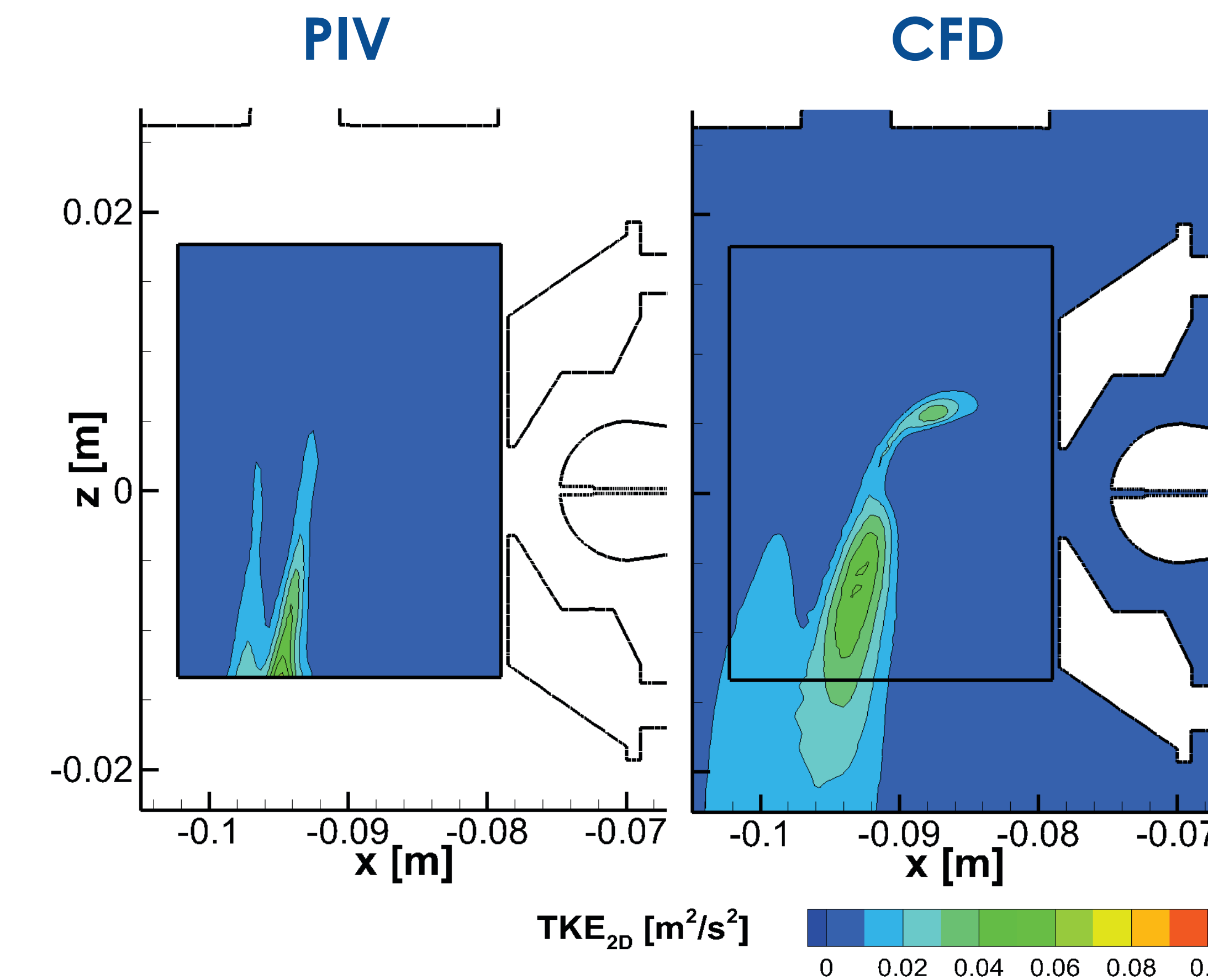


Figure 4) 2D turbulence (PIV vs. CFD)

Flow at operation point of the MPIS

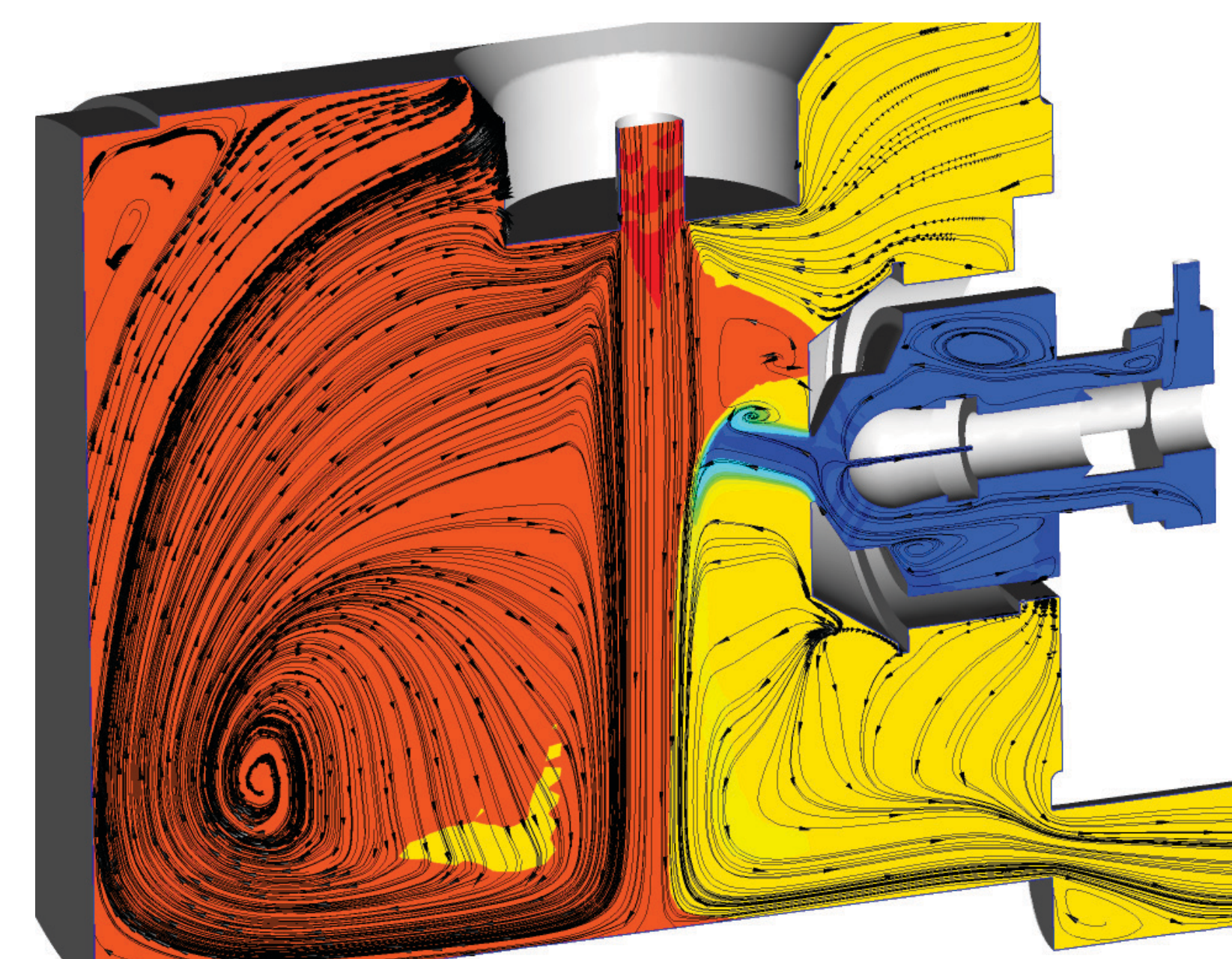
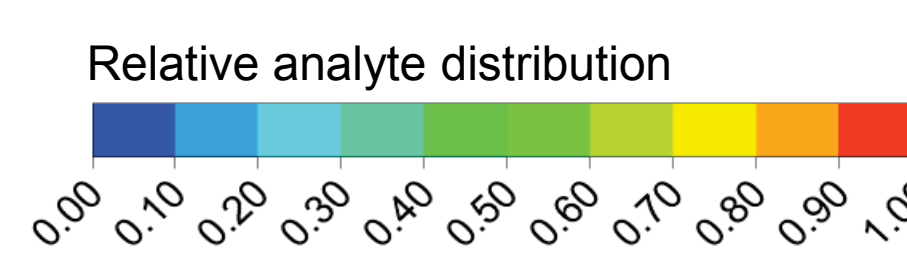


Figure 5) 2D flow pattern within the ion source

In figure 5 the two-dimensional flow pattern in the mid section of the ion source is presented. It shows a strongly inhomogeneous velocity vector distribution. The deflection of the analyte gas jet at the bottom enforces the generation of a large-scale vortex in the left part of the ion source. Since only the right-hand side of the analyte gas jet is fed by dry-gas strong mixing of dry-gas and analyte gas is not taking place. Therefore the vortex supports a higher concentration of analyte gas in the left part of the ion source.

A second, small-scale vortex is present on the top of the dry-gas jet. This is the result of an effect known from torus-shaped smoke-rings. In this case, the torus-shape is broken by the analyte gas jet (see section "Neutral Analyte distribution" for details).



Neutral Analyte Distribution

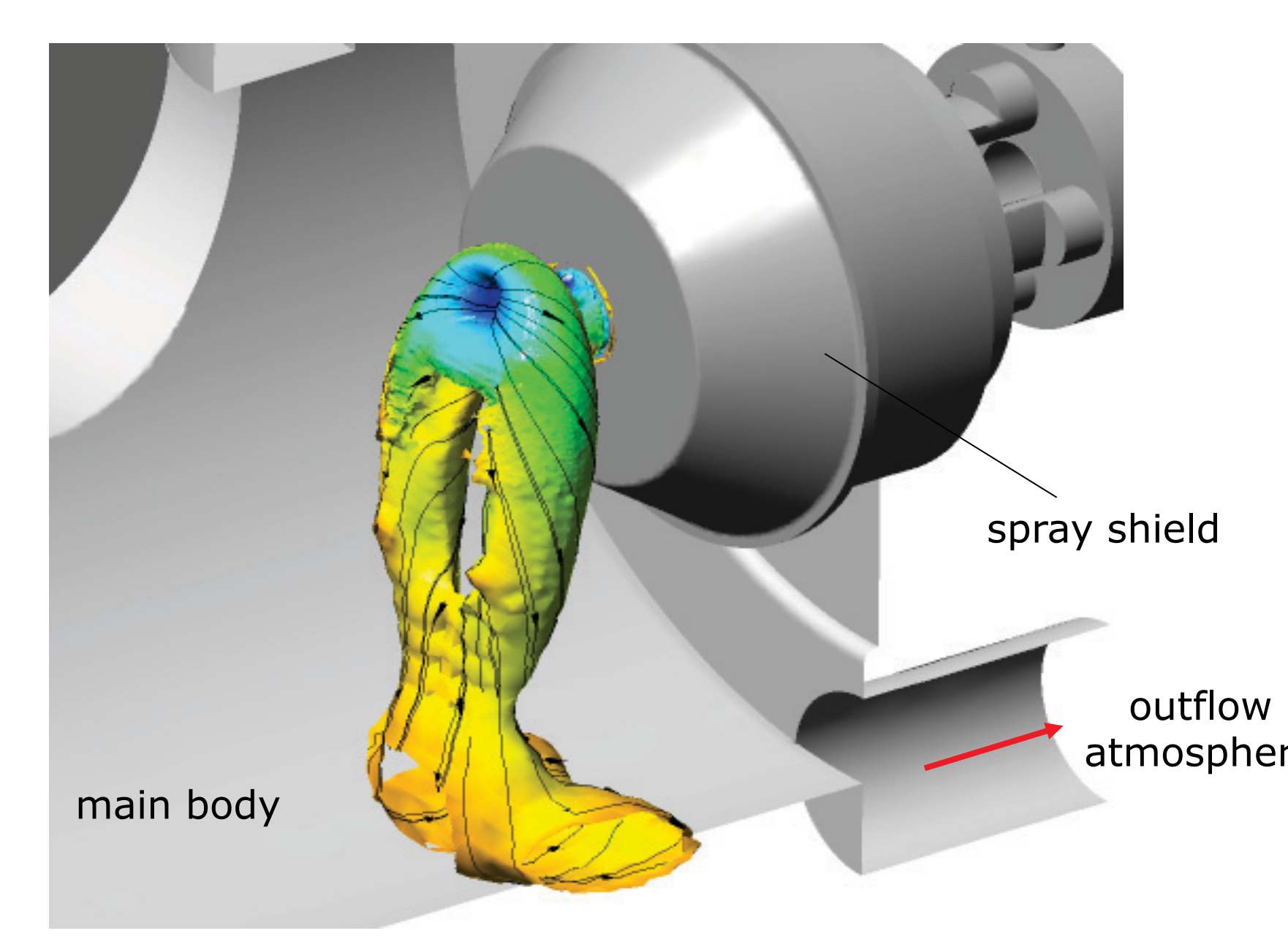
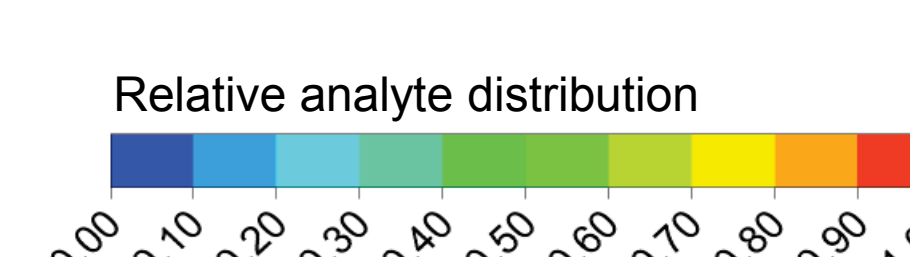


Figure 6) Horse-shoe shaped vortex in front of spray-shield

The inclination of the dry-gas jet supports the generation of a horse shoe-shaped vortex, which was also discernible in the validation results. Fig. 6 shows the three dimensional shape of this vortex in terms of an isosurface of $\lambda_2 = -80 \text{ s}^{-2}$. Negative values of λ_2 characterize closed vortical regions with a pressure minimum in the vortex core. Details of the definition of λ_2 are found in [4]. The contour demonstrates the mixing of dry-gas and analyte gas enforced by this vortex. With an initial analyte concentration of 0 in the torus center, which is coherent with the core of the dry-gas jet, the analyte concentration increases due to diffusion processes and is transported towards the spray shield by the vortical motion. Thus the vortex considerably changes the concentration of analyte gas in front of the spray shield.



Conclusions

- The bulk gas flow in the multi purpose ion source was successfully modeled with numerical methods
- The numerical results were validated with particle image velocimetry. The validation shows a very good agreement between numerical and experimental results
- The simulated flow structure is very complex, particularly the mixing / convergence zone of the two governing gas jets. This area is sensitive to subtle changes of the boundary conditions under which the source is operated
- The structure and shape of the mixing zone / convergence zone is critical for the distribution of neutral analyte in front of the MS inlet
- The minimum signal intensities in spatially resolved ion measurements (DIA measurements, see Poster 064, Session TP04) are readily explained by the numerically observed neutral analyte distribution in the mixing zone of the gas streams
- The present results provide a solid basis for the simulation of ion trajectories in the MPIS

Literature

- Appelhans, A. D.; Dahl, D. A. *SIMION ion optics simulations of atmospheric pressure* Int. J. Mass Spectrom. **2005**, *244*, 1-14.
- Lai, H.; McJunkin, T. R.; Miller, C. J.; Scott, J. R.; Almirall, J. R. *The predictive power of SIMION/SDS simulation software for modeling ion mobility spectrometry instruments* Int. J. Mass Spectrom. **2008**, *276*, 1-8.
- Ferziger, J. H.; Peric, M. *Computational Methods for Fluid Dynamics*, 3rd ed.; Springer, Berlin, Germany, **2002**
- Jeong, J.; Hussain, F. *On the identification of a vortex* Journal of Fluid Mechanics, **1995**, *285*, 69-94
- Westerweel, J. *Fundamentals of digital particle image velocimetry* J. Measurement Sci. Technol. **1997**, *8*, 1379-1392.
- Menter, F. R. *Two-Equation Eddy-Viscosity Turbulence Models for Engineering Applications*. AIAA Journal **1994**, *32*, 1598-1605.
- Roache, P. J. *Quantification of Uncertainty in Computational Fluid Mechanics*. Ann. Rev. Fluid Mech. **1997**, *29*, 123-160.

Acknowledgement

Financial support is gratefully acknowledged:
DFG (BE2124/6-1 and BE2124/4-1)